Int. J. Heat Mass Transfer. Vol. 32, No. 3, pp. 477–486, 1989
Printed in Great Britain

0017–9310/89 $3.00 + 0.00
Pergamon Press plc

Experimental and theoretical studies of combined radiative and convective transfer in CO_2 and H_2O laminar flows

A. SOUFIANI and J. TAINE

Laboratoire d'Energétique Moléculaire et Macroscopique, Combustion, CNRS, Ecole Centrale des Arts et Manufactures, Grande Voie des Vignes, 92295 Chatenay-Malabry Cedex, France

(*Received* 17 *May* 1988 *and in final form* 11 *July* 1988)

Abstract—Coupled radiative and convective transfer are studied experimentally and theoretically in the case of CO_2 and H_2O laminar flows. A channel with uniform wall temperatures and a rectangular cross-section of aspect ratio equal to 5 is used. A non-intrusive optical measurement technique, based on high resolution spectroscopy of carbon monoxide, is used to measure temperature profiles at two cross-sections of the channel. This technique appears to be more precise than shielded thermocouple measurements. Optical measurements are in good agreement with the results of a previously developed model in which spectral radiative properties of the flowing gas are calculated by using a statistical narrow-band model. The agreement between theoretical and experimental results is checked for both temperature profiles and the global heat transfer between the measurement sections.

1. INTRODUCTION

IN A LARGE variety of industrial applications, knowledge of radiative transfer in flowing infra-red gases is crucial for the determination of heat fluxes on the walls of the system. These applications include rocket and aircraft engines, boilers and furnaces, nuclear reactor safety, etc. Gas to wall heat transfer in such systems results from coupled radiation and convection processes which cannot be, in general, estimated separately.

The theoretical analysis of this problem has received considerable attention during the last 25 years (see, e.g. refs. [1, 2] for a literature survey), while only few experimental investigations have been devoted to the subject. Nichols [3] first studied experimentally the effects of radiation on temperature profiles of water vapour flowing turbulently in an annular passage at two different pressures (1 and 3.22 atm) and at a Reynolds number close to 20 000. He compared successfully his measurements with theoretical predictions based on a perturbation method and assuming that radiative transfer is small when compared to turbulent convection. More recently, Greif and co-workers investigated the interaction between radiation and convection in flowing H_2O and CO_2 inside a vertical tube of 5 cm i.d. heated electrically with a constant flux. The first experiments [4, 5] were related to turbulent H_2O and CO_2 flows and another study was related to laminar CO_2 flows [6]. Temperature profiles were measured in these investigations by using thermocouples with radiation shields and the maximum temperature reached at the wall was about 670 K. Some other experimental studies [7] are limited to the measurement of radiative fluxes emitted from flames in order to model fire propagation phenomenon or to improve the predictions of radiative fluxes on the walls of combustion chambers. Emission spectra from flames have also been used for temperature and concentration measurements [8].

In this paper, coupled radiation and convection is investigated experimentally in the case of H_2O and CO_2 laminar flows inside a channel with a rectangular cross-section of aspect ratio equal to 5. The channel walls are at uniform temperatures. A non-intrusive optical temperature measurement technique, based on the inversion of the spectral shape of an infra-red absorption line, is used for the measurement of temperature profiles at two cross-sections of the channel. Experimental results are compared with theoretical predictions obtained from a previously developed model [9] where statistical narrow-band models are used for the calculation of fluid radiative properties.

The experimental setup is described in Section 2 together with the optical arrangement used for spectroscopic technique measurements. In Section 3, the basis of the theoretical model is briefly recalled and the conditions of comparison with experiments are explained. Measured and calculated temperature profiles are compared in Section 4; convective and radiative parts of the overall heat transfer are then discussed in the case of our experiments.

2. EXPERIMENTAL SETUP

2.1. *General description*

A stationary flow, open-circuit channel was designed and built for the present study. The experimental apparatus allows the study of H_2O, CO_2, CO, air flows, or a mixture of these gases, inside a channel

NOMENCLATURE

C	current intensity of the diode laser [mA]
C_p	specific heat at constant pressure [J kg^{-1} K^{-1}]
d	column length [cm]
E	distance between the channel walls, 0.03 m
$F(\nu-\nu_0)$	spectral shape of the absorption line [1/cm^{-1}]
H	enthalpy flux [W]
K_ν	spectral absorption coefficient [cm^{-1}]
L	distance between the two measurement cross-sections, 1.2 m
$\dot{m}$	mass flow rate [kg s^{-1} m^{-2}]
P	total pressure [atm]
q_{rx}, q_{ry}	axial and transverse local radiative flux components, respectively [W m^{-2}]
Re	Reynolds number
$S_0(T)$	line strength [cm^{-2} atm^{-1}]
T	temperature [K]
T_b	bulk temperature [K]
T_u, T_l	upper and lower wall temperatures, respectively [K]
u, v	axial and transverse velocity components, respectively [m s^{-1}]
x, y, z	system coordinates [m]
x_j	molar fraction of species j
Z	channel width, 0.15 m.

Greek symbols

β_{aj}	temperature dependence coefficient of a Lorentz half-width
ε_w	wall emissivity
γ	Lorentz half-width (HWHM) [cm^{-1}]
φ_{cd}	conductive flux transferred from the walls to the gas [W m^{-2}]
φ_r	radiative flux transferred from the walls to the gas [W m^{-2}]
λ	thermal conductivity [W m^{-1} K^{-1}]
μ	viscosity [kg m^{-1} s^{-1}]
ν	radiation wave number [cm^{-1}]
ν_0	line centre wave number [cm^{-1}]
ρ	density [kg m^{-3}]
τ_ν	spectral transmissivity.

of rectangular cross-section. The apparatus is schematically shown in Fig. 1. Water vapour is produced in an electrical steam generator working at a regulated pressure (about 6 bar), while CO_2 and CO are supplied from pressurized gas tanks ('Air Liquide', pure gases). The partial flow rate of each species is measured using orifice flowmeters. The flowing mixture is then heated electrically before entering the test section. The temperature reached at the channel entrance can be varied from 300 to 1000 K depending on the working conditions. The flow is mechanically conditioned inside a plenum chamber which includes a honeycomb and a convergent duct with a ratio between the upstream and downstream sections equal to 6.6.

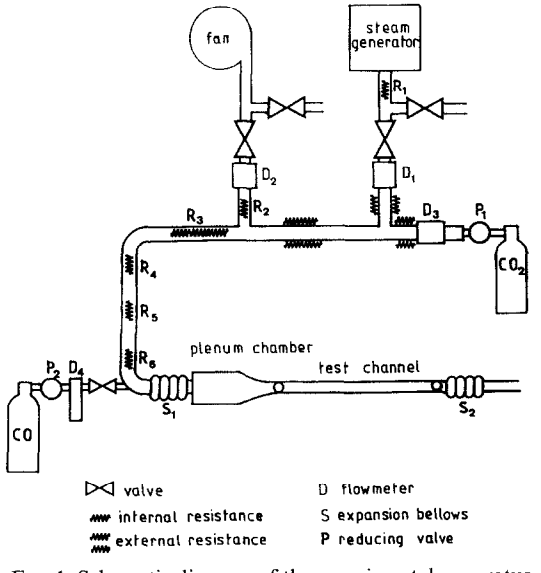

FIG. 1. Schematic diagram of the experimental apparatus.

A schematic view of the horizontal test channel is given in Fig. 2. Its total length is 2 m and the aspect ratio of its cross-section is equal to 5 (15 cm wide and 3 cm high). The channel is made of four stainless steel walls which are assembled in such a manner that optical measurements can be carried out for any beam position close to the horizontal walls (Fig. 3). The upper and lower channel walls are at uniform but different temperatures. The upper wall is heated electrically by 16 flat resistances monitored by an Apple II microcomputer. The temperature under each resistance is held at a fixed value T_u in the 350–950 K range. The lower wall is held at a temperature T_l close to 373 K using a liquid–vapour water phase change. This asymmetric configuration is used for two reasons:

(a) it avoids flow instabilities and recirculations due to natural convection in the case of laminar flows;

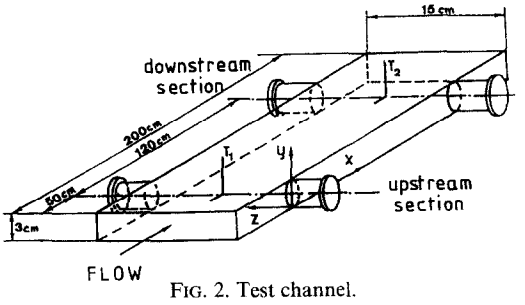

FIG. 2. Test channel.

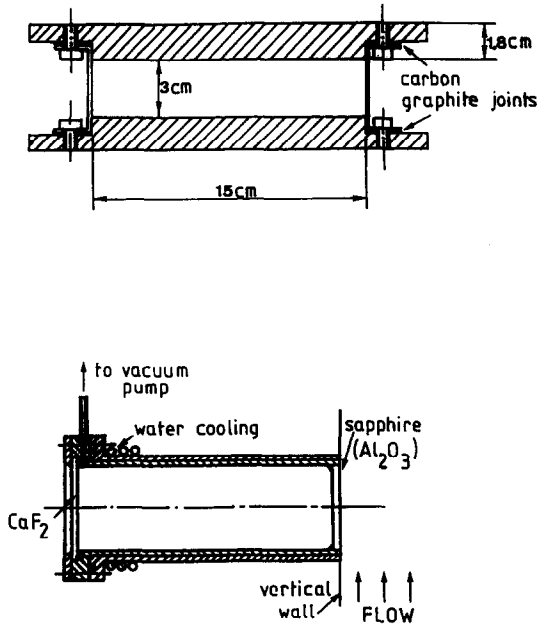

FIG. 3. Channel cross-section and optical window assembly.

(b) this arrangement results in a minimal perturbation of measurements due to thermal boundary layers on the vertical channel walls.

Deviations from the fixed wall temperatures are given by 25 chromel–alumel thermocouple measurements. The maximum deviations are about ± 5 K for T_1 and ± 10 K at 400 K and ± 18 K at 800 K for T_u. Four windows enable optical measurements at two cross-sections of the channel 1.20 m away from one another (Fig. 2). Each window includes a sapphire (Al_2O_3) slab brazed on titanium, in line with the inside vertical surface of the channel (with 0.1 mm tolerance, in order to avoid flow perturbations), and a CaF_2 slab on the other side (Fig. 3). The enclosure between Al_2O_3 and CaF_2 slabs is under vacuum in order to minimize laser beam perturbations due to natural convection outside the channel. Measurements at the upstream section are introduced as inlet conditions in the parabolic flow calculations while measurements at the downstream section are compared with the results of these calculations (Section 4).

2.2. *Instrumentation*

Only temperature profiles are measured at the two cross-sections of the channel. In fact, it appears that the shape of the velocity profile at the upstream section has no influence on the calculated temperature profile at the downstream section, as will be discussed in Section 3.

Temperature is measured using both a classical probe technique and an original optical technique. Thermocouples (1 mm chromel–alumel) with radiation shields are used for measurements 3 cm away from the optical sections of the channel. Thermocouples are micrometric screw displaced in the flow and the radiation shields are retracted in the upper wall of the channel before proceeding to optical measurements. The accuracy of thermocouple measurements is discussed in Section 4.

The spectroscopic technique used here is based on the inversion of the spectral shape of a vibration–rotation line, obtained from an absorption setup and a diode laser as infra-red source. A similar technique has been applied by Hanson and his co-workers [10, 11] to measure the concentration of molecular species such as CO and NO in combustion media. Temperature in such media can be deduced from the ratio of the strengths of two nearly coincident absorption lines, characterized by different lower energy levels [12]; this is particularly suitable for high temperature measurements. For intermediate temperatures (300–1000 K), it seems more judicious to use the temperature dependence of the Lorentz half-width of an absorption line.

2.2.1. *Basis and calibration of the spectroscopic technique.* The spectral transmissivity τ_ν of a homogeneous and isothermal gaseous column of length d is given by

$$\tau_\nu = \exp(-K_\nu d) \tag{1}$$

where K_ν is the spectral absorption coefficient defined for an isolated line of the absorbing species a, centred at wave number ν_0, by

$$K_\nu = K_{\nu 0}(\nu) = x_a P S_0(T) F(\nu - \nu_0). \tag{2}$$

Here x_a designates the molar fraction of species a, P the total pressure, $S_0(T)$ the line strength at temperature T and $F(\nu-\nu_0)$ the normalized line shape. In our experimental conditions ($300\ \text{K} \leqslant T \leqslant 1000$ K and $P = 1$ atm), the line broadening is mainly due to molecular collisions and Doppler effects can be neglected. The line shape is then a Lorentzian one

$$F(\nu-\nu_0) = \gamma/(\pi(\gamma^2 + (\nu-\nu_0)^2)) \tag{3}$$

it is characterized by the Lorentz half-width γ(HWHM) which depends on total pressure, temperature and molar fractions x_j of all the mixture components

$$\gamma = \sum_{\text{species } j} x_j (P/P_s) \gamma_{aj}(T_s)(T_s/T)^{\beta_{aj}}. \tag{4}$$

$\gamma_{aj}(T_s)$ is the Lorentz half-width of the absorption line broadened by collisions with partner j under standard temperature and pressure conditions; β_{aj} designates the temperature power law dependence coefficient.

Measurements of absorption spectra around wave number ν_0 enable the determination of the quantities $x_a S_0(T)$ and γ. The temperature of the isothermal path length and concentration of the absorbing species can then be deduced from these parameters if the coefficients $\gamma_{aj}(T_s)$ and β_{aj} are known. In our experiments, the absorbing species is diluted in the flowing gas with a molar fraction lower than 10^{-2}. The precise knowledge of x_a is not required for temperature determination from the Lorentz half-width since the con-

Table 1. Collisional broadening of the 1-0 P(4) CO line; parameters to be used with equation (5) and $T_s = 300$ K

Collision partner, j	$\gamma_{CO-j}(T_s)$ (cm^{-1} atm^{-1})	β_{CO-j}
N_2	0.069	0.690
H_2O	0.104	0.740
CO_2	0.0925	0.667

tribution of self-broadening is then negligible when compared with that of foreign-broadening (equation (4)). The absorbing species chosen in this study is carbon monoxide which presents the following advantages.

(1) CO vibration–rotation lines are well resolved (the rotational constant is $B_v \approx 1.92$ cm^{-1}); no overlapping line effects are to be accounted for in the data reduction procedures.

(2) The total absorbtance of the CO fundamental band is sufficiently small; heat transfer in transparent gases can be studied without adding CO radiation effects.

The particular absorption line used is the P(4) line of the fundamental band, centred at $\nu_0 = 2127.693$ cm^{-1}. Infra-red active molecules such as CO_2 and H_2O are transparent at this wave number for temperatures lower than 1500 K.

The calibration of this spectroscopic technique requires the measurement of the temperature dependence of the CO-P(4) broadening coefficients due to different species. These measurements have been performed on a high temperature spectroscopic setup for CO–N_2, CO–H_2O and CO–CO_2 mixtures inside thermally stabilized cells [13–15]. The measured values of γ_{CO-j} in the temperature range 293–900 K can be approximated within 2% by the power law

$$\gamma_{CO-j}(T) = \gamma_{CO-j}(T_s)(T_s/T)\beta_{CO-j}. \quad (5)$$

The values of $\gamma_{CO-j}(T_s)$ and β_{CO-j} for $j = N_2$, H_2O and CO_2 are given in Table 1. Further details of these measurements and comparisons with theoretical predictions are available in refs. [13–15].

2.2.2. *Optical setup and data reduction procedures.* A schematic view of the optical setup is given in Fig. 4. The diode laser beam is mechanically chopped and enters a grating monochromator which selects a single emission mode. It is then split in three parts. The first beam is directly focused on the detector D1 and enables the recording of variations of the laser radiation intensity. The second beam goes through a reference cell containing a CO–N_2 etalon mixture at room temperature. The transmissivity of this mixture leads to the conversion law between radiation frequency variations and the diode current C. The third beam is split in two equal parts in order to sound the flow at the two cross sections of the channel. Four motorized units, including step by step motors, allow pre-

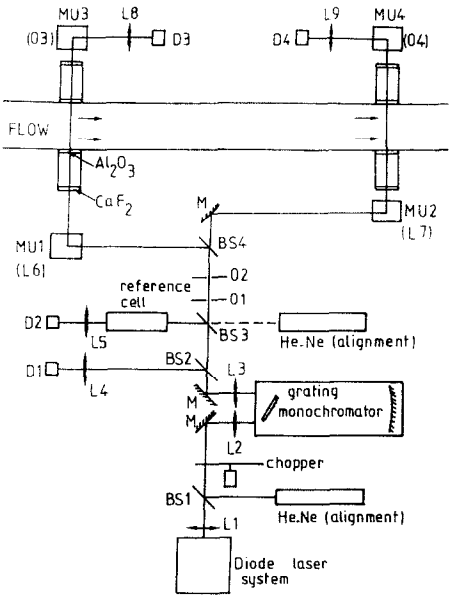

FIG. 4. Optical setup for diode-laser measurements: M, Au mirror; L, CaF_2 lens; BS, CaF_2 beam splitter; O, diaphragm; D, detector; MU, motorized unit for vertical displacements.

cise vertical displacements of the beams with 1 μm resolution.

The four chopped signals delivered by the detectors are filtered in lock-in amplifiers and digitalized together with the diode laser current by a 12 bits A/D conversion card of a PDP 11-23 computer. Numerical averaging of the converted values is made for each radiation frequency.

The spectral absorption coefficient is deduced from two experiments. The first is performed with the flowing gas seeded with CO and the reference cell filled with the etalon CO–N_2 mixture. The second is performed with an empty reference cell and without CO in the flow. The ratio between the signals recorded during these experiments leads to the transmissivity vs the diode current and then vs radiation frequency. A non-linear least-squares fitting of the measured absorption spectra by the theoretical Lorentz shape leads to the determination of the Lorentz half-width and then to temperature using equation (5) and the calibration parameters of Table 1. Figure 5 shows an example of measured profiles for a water vapour flow and corresponding theoretical fits. Agreement between the two spectra is very good.

This optical technique has been previously applied to the study of laminar channel air flows [16]. The measurement uncertainties have been estimated to $\pm 2\%$ at 300 K and $\pm 3\%$ at 900 K.

3. THEORETICAL PREDICTIONS AND CALCULATION PARAMETERS

In a previously published study [9], the interaction between radiation and convection in channel flows has been investigated theoretically. The same analysis

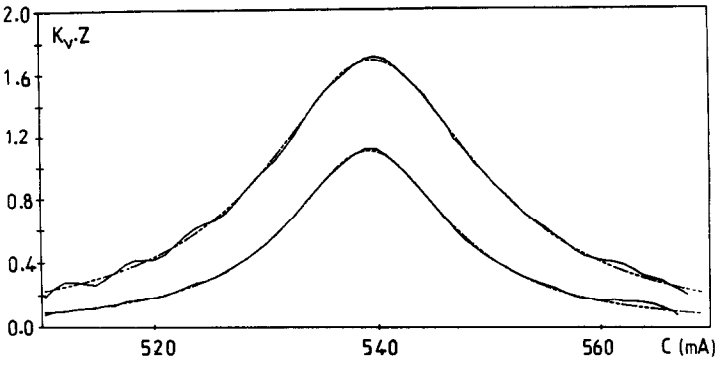

FIG. 5. Typical spectral line profiles recorded at the downstream section for a water vapour flow: ———, measured spectra; – – – –, best fit by a Lorentz profile. C designates the diode current which is a monotonous function of radiation frequency.

is used here to make comparisons with experimental results. Theoretical basis and numerical procedures are briefly recalled in Section 3.1, and the calculation parameters are given in Section 3.2.

3.1. *Theoretical basis*

The two-dimensional form of the mass, momentum and enthalpy balance equations are

$$\frac{\partial}{\partial x}(\rho u) + \frac{\partial}{\partial y}(\rho v) = 0 \tag{6}$$

$$\rho u \frac{\partial u}{\partial x} + \rho v \frac{\partial u}{\partial y} = -\frac{\partial P}{\partial x} + \frac{\partial}{\partial y}\left(\mu \frac{\partial u}{\partial y}\right) \tag{7}$$

$$\rho C_p u \frac{\partial T}{\partial x} + \rho C_p v \frac{\partial T}{\partial y} = \frac{\partial}{\partial y}\left(\lambda \frac{\partial T}{\partial y}\right) - \frac{\partial q_{ry}}{\partial y} \tag{8}$$

where u and v are the axial and transverse velocity components, respectively. ρ, μ, λ and C_p designate the temperature-dependent density, viscosity, thermal conductivity and specific heat at constant pressure, respectively. q_{ry} is the transverse component of the radiative flux vector. It is assumed here that the axial radiative dissipation term $\partial q_{rx}/\partial x$ is negligible when compared with the transverse dissipation $\partial q_{ry}/\partial y$ [17] as it is usually done for the conductive dissipation in the case of parabolic flows. Radiative properties of CO_2 and H_2O are calculated by using a random statistical narrow-band model to account for the high resolution structure of the absorption spectra. For these two molecules, and especially at high temperature, the most accurate model is that where line intensities obey an exponential-tailed-inverse distribution law [18]. This model is used in this study together with the Curtis–Godson approximation for non-isothermal paths. It leads to temperature and flux distributions more accurate than those predicted by the exponential wide-band model [9].

The governing flow and energy equations are solved simultaneously in order to account for the temperature dependencies of density and viscosity. An implicit finite difference scheme is used to solve the flow equations, following the recommendations of Patankar [19]. The radiative dissipation term $\partial q_{ry}/\partial y$ is computed by integration over the absorption spectra and the propagation directions. A direct radiative balance is carried out for each control volume. Further details on the numerical procedure and derivation of the radiative dissipation term are given in ref. [9]. The same analysis is used here, except for the two wall radiosities which are not equal in this study. Equation (30) of ref. [9] is replaced by

$$B_1^k = \varepsilon_{\nu^k}\pi\Delta\nu I_{\nu^k}^b(T_1) + (1-\varepsilon_{\nu^k}) \sum_{j=2}^{N} A_{1j}^k B_j^k \tag{9}$$

$$B_N^k = \varepsilon_{\nu^k}\pi\Delta\nu I_{\nu^k}^b(T_u) + (1-\varepsilon_{\nu^k}) \sum_{j=1}^{N-1} A_{jN}^k B_j^k \tag{10}$$

where subscripts 1 and N designate the lower and upper walls, respectively.

3.2. *Calculation parameters*

Thermophysical properties of the studied gases can be approximated by a temperature dependence law

$$Z = G + FT^m \tag{11}$$

within a 2% maximum error in the temperature range 300–1000 K. The values of G, F and m for λ, μ and C_p have been deduced from a compilation of different data [20, 21]. These values are given in Table 2 for H_2O and CO_2. The state equation for a perfect gas is used to calculate density.

The statistical narrow-band model is used with 25 cm^{-1} spectral resolution. The parameters of this model, generated from a line by line calculation (see, e.g. ref. [18]), are stored at intermediate temperatures and a simple interpolation is used for any temperature. Seventy-two narrow bands are considered for the 2.7, 4.3 and 15.2 μm vibration–rotation bands of CO_2. For H_2O, 140 narrow bands are considered, covering the 2.7 and 6.3 μm vibration–rotation bands and the pure rotation band which is truncated at 70 μm.

The spectral directional emissivity of the stainless steel used for the channel walls has been measured at different wavelengths in the range 3–10 μm and at different temperatures in the 300–800 K range. The

Table 2. Thermophysical properties of H_2O (subscript 1) and CO_2 (subscript 2); to be used with equation (11)

Z	Unit	F	G	m
λ_1	$W\,m^{-1}\,K^{-1}$	-0.0166	1.05×10^{-4}	1
λ_2	$W\,m^{-1}\,K^{-1}$	-6.26×10^{-3}	7.626×10^{-5}	1
μ_1	$10^{-6}\,kg\,m^{-1}\,s^{-1}$	-3.071	0.0407	1
μ_2	$10^{-6}\,kg\,m^{-1}\,s^{-1}$	-14.93	1.728	0.5
C_{p1}	$J\,kg^{-1}\,K^{-1}$	1680	0.600	1
C_{p1}	$J\,kg^{-1}\,K^{-1}$	20	166.0	0.287

Table 3. Experimental conditions for H_2O and CO_2 flows: T_u, upper wall temperature; T_l, lower wall temperature

Experiment	Fluid	Figure	T_u (K)	T_l (K)	$\dot{m}$ ($kg\,m^{-2}\,s^{-1}$)	Re $x=0$	Re $x=L$
H1	H_2O	6	623	383	0.390	1583	1426
C1	CO_2	7	623	360	0.294	1144	1072
C2	CO_2	8	723	383	0.383	1588	1448
C3	CO_2	9	783	378	0.356	1471	1329

apparatus used for these measurements is described in ref. [22]. No significant variations have been observed when the probe temperature varied. In the same manner, variations lower than 10% are obtained when varying the wavelength or the angle between the emission direction and the normal to the probe in the 0°–70° range. The direction and wavelength averaged emissivity was found to be $\varepsilon_w = 0.27$. This value is assumed in the numerical predictions to be independent of temperature, wavelength and emission direction (diffuse and gray walls).

The last conditions required for solving the parabolic flow equations are the inlet conditions ($x = 0$, upstream section). The inlet temperature profile is given by diode laser measurements at the upstream section. For the axial velocity, the inlet profile is assumed to be parabolic and is calculated from orifice flowmeter measurements in such a manner that the total flow rate is conserved. Calculations using a flat velocity profile at $x = 0$ lead to a maximum temperature difference lower than 1 K at the downstream section. The important dynamical quantity is the mass flow rate rather than the velocity profile.

4. RESULTS AND DISCUSSION

Diode laser measurements presented below are averages of temperatures obtained from two line records and the error bands indicate a confidence interval of $\pm 2.5\%$ due to measurement uncertainties. Four experiments of radiating gas flows are reported in this paper. The first refers to a H_2O flow while the three others are related to CO_2 flows with increasing upper wall temperature in order to increase radiative transfer. Table 3 shows the flow conditions related to each experiment. The Reynolds number given in this table is based on the bulk temperature T_b

$$Re = 2E\dot{m}/\mu(T_b) \tag{12}$$

and then varies with x. $\dot{m}$ designates the mass flow rate per unit cross-sectional area

$$\dot{m} = (1/E)\int_0^E \rho u\,dy. \tag{13}$$

The bulk temperature at the upstream section is chosen in our experiments close to the cold wall temperature in order to produce a significant increase of the total enthalpy flux between the two measurement sections.

Figures 6–9 show the measured and calculated tem-

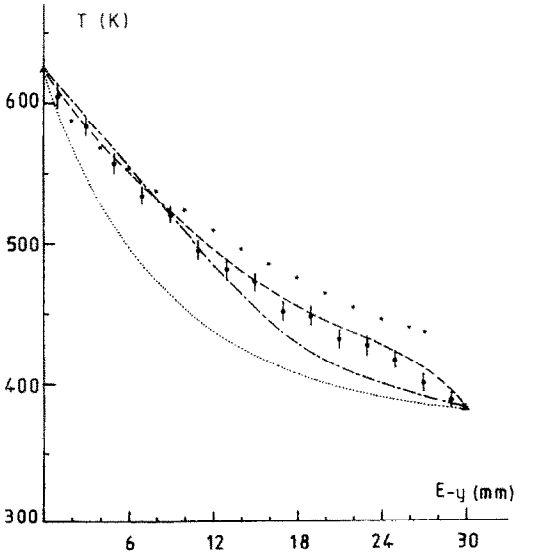

FIG. 6. Measured and calculated temperature profiles at the downstream section. Experiment H1: *, thermocouple with radiation shield measurements; ♦, diode laser measurements; ▲, constant wall temperatures; ———, calculated temperature profile at the downstream section, accounting for radiation; — — — —, calculated temperature profile at the downstream section, without radiation; ·····, diode laser measurements at the upstream section (inlet conditions).

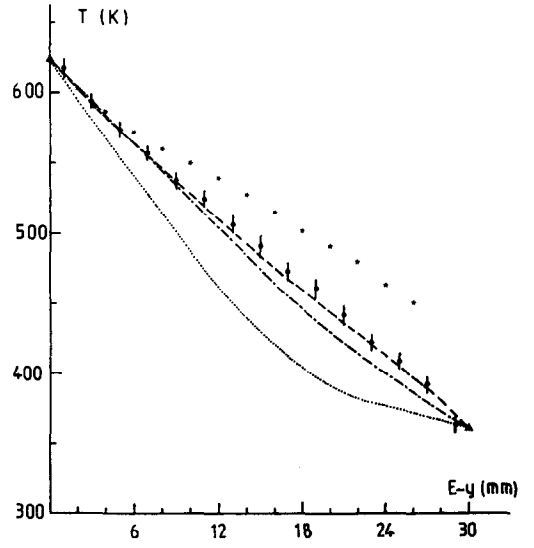

FIG. 7. Same as in Fig. 6; experiment C1.

perature profiles; five profiles are plotted on each figure.

(1) Diode laser measured profile at the upstream section.

(2) Thermocouple measured profile at the downstream section.

(3) Diode laser measured profile at the downstream section.

(4) The calculated profile accounting for coupled radiation and convection.

(5) The calculated profile without radiation effects.

Discrepancies up to 80 K between the thermocouple with radiation shield and diode laser measurements are observed, especially for high values of T_u and in the cold region of the flow. Thermocouple measurements in this region do not tend to the cold wall temperature. These discrepancies are due to the effects of hot wall radiation on the equilibrium temperature of the probe. Convective transfer between the thermocouple and the flowing gas is small in the case of laminar flows and radiation effects remain appreciable in spite of the use of radiation shields.

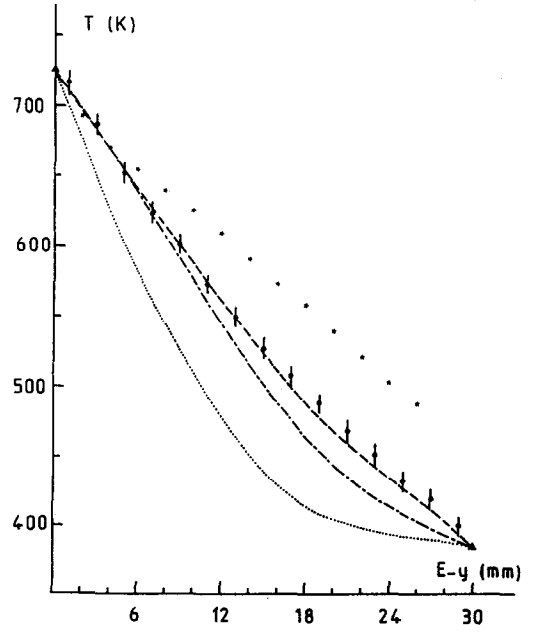

FIG. 8. Same as in Fig. 6; experiment C2.

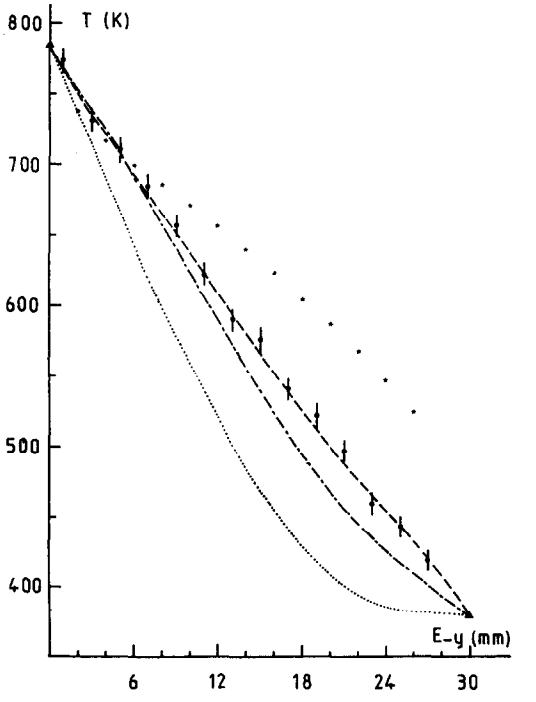

FIG. 9. Same as in Fig. 6; experiment C3.

For the water vapour experiment, the agreement between diode laser measurements and calculations is quite good but the theoretical curve does not go systematically through the error bands. In fact, the mass flow rate was not constant during H_2O experiments; $\dot{m}$ fluctuations up to $\pm 15\%$ were observed as a result of interruptions in the pressure regulation mode inside the electrical steam generator. On the other hand, CO_2 was supplied from gas tanks at constant pressure, which leads to a constant flow rate within $\pm 1\%$ during an experiment. The agreement between diode laser measurements and calculations (accounting for radiation) is then excellent for CO_2 flows.

For similar wall temperature conditions, radiation effects on the temperature profile at the downstream section are more important in the case of H_2O (Figs. 6 and 7). There are two reasons for this:

(a) the spectral widths and total absorbtances of the H_2O absorption bands are generally greater than those of CO_2;

(b) the H_2O absorption band centred at 6.3 μm is close to the maximum emission spectral range of a wall at 623 K.

Table 4. Enthalpy fluxes at the measurement sections: $H(0)$, measured at the upstream section; $H_c(L)$, calculated at the downstream section ($L = 1.2$ m); $H_m(L)$, measured at the downstream section

Experiment	$H(0)/Z$ (W m^{-1})	$H_c(L)/Z$ (W m^{-1})	$H_m(L)/Z$ (W m^{-1})	$\frac{H_m(L)-H_c(L)}{H_c(L)-H(0)}$ (%)	$\frac{H_m(L)-H_c(L)}{H_c(L)}$ (%)
H1	9745	10989	10731	−20.7	−2.3
C1	3730	4221	4218	−0.4	−0.1
C2	5140	6119	6126	0.7	0.1
C3	5084	6224	6186	−3.4	−0.6

For high values of the upper wall temperature, radiative transfer becomes important even for CO_2 flows (experiment C3). The maximum difference between the profiles calculated with and without radiation is 34 K in the case of Fig. 9.

The overall heat transfer between the measurement sections can be characterized by the difference between enthalpy fluxes at these sections. The enthalpy flux $H(x)$ is given by

$$H(x) = Z\int_0^E \rho(x,y)u(x,y)\left(\int_0^{T(x,y)} C_p(T)\,\mathrm{d}T\right)\mathrm{d}y \tag{14}$$

where Z designates the channel width (15 cm). The conductive and radiative parts of the global transfer between the flow and the walls are given, per unit wall area, by

$$\varphi_{cd}(x) = -(\lambda\partial T/\partial y)_{y=0} + (\lambda\partial T/\partial y)_{y=E} \tag{15}$$

$$\varphi_r(x) = q_{ry}(0) - q_{ry}(E) = \int_0^E -\partial q_{ry}/\partial y\,\mathrm{d}y. \tag{16}$$

The difference between the enthalpy fluxes at the measurement sections is obtained from an integration of the energy equation over the studied volume

$$(1/Z)(H(L)-H(0)) = \int_0^L (\varphi_{cd}(x)+\varphi_r(x))\,\mathrm{d}x. \tag{17}$$

Table 4 gives the values of H deduced from diode laser measurements and equation (14) at the two sections, and the calculated values at the downstream section. The agreement between predicted and measured global heat transfer values is very good for CO_2 flows (<3.4%), while discrepancies similar to the uncertainties on the flow rate $\dot{m}$ are obtained for the H_2O flow. The conductive and radiative fluxes, calculated at different sections $0 \leqslant x \leqslant L$, are shown in Fig. 10 for experiments H1 and C3. Radiative transfer reaches approximately 30% of the conductive transfer in the case of CO_2 at $x = L$, and 50% in the case of H_2O.

5. CONCLUSIONS

A rectangular test channel with uniform wall temperatures has been designed to study coupled convection and radiation in internal H_2O and CO_2 laminar flows. Both classical shielded thermocouple and original optical techniques have been used to measure temperature profiles at two cross-sections of the channel. The optical technique is based on the inversion of the spectral shape of the 1-0 P(4) CO absorption line, and particularly on the temperature dependence of the Lorentz width of this line. This non-intrusive technique appeared to be more precise than the classical probe technique since the latter is sensitive to wall radiation, in spite of the use of radiation shields. Optical measurements have been compared with the results of a previously developed model where absorption and emission are taken into account by using a statistical narrow-band model and our parameters. The optical measurements at the upstream section have been used as inlet conditions in the parabolic flow calculations. A very good agreement between measured and calculated profiles is obtained, especially in the case of CO_2 flows for which satisfactory experimental conditions were checked. The measured global heat transfer between the channel

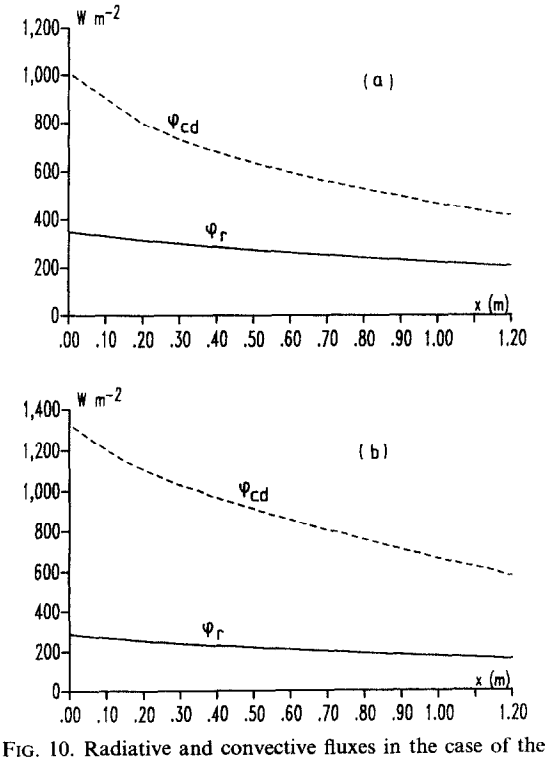

FIG. 10. Radiative and convective fluxes in the case of the H1 (a) and C3 (b) experiments.

walls and the flow has been also successfully compared with numerical predictions. The influence of radiation on temperature profiles and enthalpy fluxes has been clearly demonstrated in the case of CO_2 and H_2O laminar flows.

REFERENCES

1. R. Viskanta, Radiative heat transfer: interaction with conduction and convection and approximate methods in radiation, *Proc. 7th Int. Heat Transfer Conf.*, Munich, Vol. 1, p. 103 (1982). See also: Radiative heat transfer, *Fortschr. Verfahrenstech.* **22,** 51 (1984).
2. R. Viskanta and P. Mengüc, Radiation heat transfer in combustion systems, *Proc. Energy Combust. Sci.* **13,** 97 (1987).
3. L. D. Nichols, Temperature profile in the entrance region of an annular passage considering the effects of turbulent convection and radiation, *Int. J. Heat Mass Transfer* **8,** 589 (1965).
4. I. S. Habib and R. Greif, Heat transfer to a flowing non-gray radiating gas: an experimental and theoretical study, *Int. J. Heat Mass Transfer* **13,** 1571 (1970).
5. Z. Chiba and R. Greif, Heat transfer to steam flowing turbulently in a pipe, *Int. J. Heat Mass Transfer* **16,** 1645 (1973).
6. R. Greif, Laminar convection with radiation: experimental and theoretical results, *Int. J. Heat Mass Transfer* **21,** 477 (1978).
7. S. M. Jeng and G. M. Faeth, Species concentrations and turbulence properties in buoyant methane diffusion flames, *J. Heat Transfer* **106,** 721 (1984). See also: E. S. Fishburne and H. S. Pergament, The dynamics and radiant intensity of large hydrogen flames, 17th Symposium (International) on Combustion, pp. 1063–1073, Pittsburg, Pennsylvania (1979).
8. C. C. Ferriso, C. B. Ludwig and F. P. Boynton, A band-ratio technique for determining temperatures and concentrations of hot combustion gases from infrared-emission spectra, 10th Symposium (International) on Combustion, pp. 161–175, Pittsburg, Pennsylvania (1965).
9. A. Soufiani and J. Taine, Application of statistical narrow-band model to coupled radiation and convection at high temperature, *Int. J. Heat Mass Transfer* **30,** 437 (1987).
10. S. M. Schoenung and R. K. Hanson, CO and temperature measurements in a flat flame by laser absorption spectroscopy and probe techniques, *Combust. Sci. Technol.* **24,** 227 (1981).
11. P. K. Falcone, R. K. Hanson and C. H. Kruger, Tunable diode laser absorption measurements of nitric oxide in combustion gases, *Combust. Sci. Technol.* **35,** 81 (1983).
12. R. K. Hanson and P. K. Falcone, Temperature measurement technique for high temperature gases using a tunable diode laser, *Appl. Opt.* **17,** 2477 (1978).
13. J. M. Hartmann, M. Y. Perrin, J. Taine and L. Rosenmann, Diode-laser measurements and calculations of CO 1-0 P(4) line broadening in the 294- to 765-K temperature range, *J. Quant. Spectrosc. Radiat. Transfer* **35,** 357 (1986).
14. A. Soufiani and J. M. Hartmann, Measurements and calculations of CO–H_2O line-widths at high temperature, *J. Quant. Spectrosc. Radiat. Transfer* **37,** 205 (1987).
15. A. Soufiani and L. Rosenmann, Diode-laser measurements and calculations of CO–CO_2 line-widths at high temperature, *J. Quant. Spectrosc. Radiat. Transfer* **39,** 441 (1988).
16. A. Soufiani and J. Taine, Diode laser temperature measurements and calculations in nonisothermal channel air flows, *Proc. First World Conf. on Experimental Heat Transfer, Fluid Mechanics and Thermodynamics*, Dubrovnik (September 1988).
17. S. De Soto, Coupled radiation, conduction, and convection in entrance region flow, *Int. J. Heat Mass Transfer* **11,** 39 (1968).
18. A. Soufiani, J. M. Hartmann and J. Taine, Validity of band-model calculations for CO_2 and H_2O applied to radiative properties and conductive–radiative transfer, *J. Quant. Spectrosc. Radiat. Transfer* **33,** 243 (1985).
19. S. V. Patankar, *Numerical Heat Transfer and Fluid Flow*. Hemisphere, New York (1980).
20. R. C. Reid and T. K. Sherwood, *The Properties of Gases and Liquids*, Chemical Engineering Series, 2nd Edn. McGraw-Hill, New York (1966).
21. Y. S. Touloukian, P. E. Liley and S. C. Saxena, *Thermophysical Properties of Matter*, Vol. 3. IFI/Plenum, New York/Washington (1970); Y. S. Touloukian, S. C. Saxena and P. Hestermans, *Thermophysical Properties of Matter*, Vol. 11. IFI/Plenum, New York/Washington (1970).
22. J. M. Ané and M. Huetz-Aubert, Stratified media theory interpretation of measurements of the spectral polarized directional emissivity of some oxidized metals, *Int. J. Thermophys.* **7,** 1191 (1986).

ETUDES EXPERIMENTALE ET THEORIQUE DES TRANSFERTS COUPLES PAR CONVECTION ET RAYONNEMENT DANS DES ECOULEMENTS LAMINAIRES DE CO_2 ET H_2O

Résumé—Les transferts couplés par convection et rayonnement sont étudiés expérimentalement et théoriquement dans le cas d'écoulements laminaires de CO_2 et H_2O. Un canal à températures de parois constantes, caractérisé par une section droite de rapport d'allongement égal à 5, est utilisé. Une technique non-intrusive optique, fondée sur la spectroscopie à haute résolution du monoxyde de carbone, est utilisée pour mesurer les champs de température en deux sections droites du canal. Cette technique s'avère beaucoup plus précise que celle utilisant des thermocouples à écrans radiatifs. Les mesures optiques sont en bon accord avec les résultats d'un modèle developpé antérieurement, où les propriétés radiatives du gaz en écoulement sont calculées à partir d'un modèle statistique à bandes étroites. L'accord entre les résultats théoriques et expérimentaux est obtenu aussi bien pour les profils de température que pour le transfert global de chaleur entre les sections de mesure.

EXPERIMENTELLE UND THEORETISCHE UNTERSUCHUNGEN DES WÄRMEAUSTAUSCHES DURCH STRAHLUNG UND KONVEKTION IN LAMINAREN CO_2- UND H_2O-STRÖMUNGEN

Zusammenfassung—Der Wärmeaustausch durch Strahlung und Konvektion wird experimentell und theoretisch für laminare CO_2- und H_2O-Strömungen untersucht. Verwendet wurde ein rechteckiger Strömungskanal mit gleichförmiger Wandtemperatur und einem Seitenverhältnis von 5. Zur Messung der Temperaturverteilung an zwei verschiedenen Kanalquerschnitten wurde eine optische Meßmethode verwendet, die auf einer hochauflösenden Kohlenmonoxid-Spektroskopie basiert. Diese Technik scheint genauere Meßergebnisse zu liefern, als Messungen mit strahlungsgeschützten Thermoelementen. Die optischen Messungen stimmen gut mit den Ergebnissen eines früher entwickelten Rechenverfahrens überein, in welchem die spektralen Strahlungseigenschaften des Gases mit einem statistischen Schmalband-Modell berechnet werden. Die Übereinstimmung zwischen theoretischen und experimentellen Ergebnissen wurde sowohl für die Temperaturprofile als auch den globalen Wärmetransport zwischen den Meßquerschnitten überprüft.

ЭКСПЕРИМЕНТАЛЬНОЕ И ТЕОРЕТИЧЕСКОЕ ИССЛЕДОВАНИЕ СОВМЕСТНОГО ЛУЧИСТОГО И КОНВЕКТИВНОГО ПЕРЕНОСА ПРИ ЛАМИНАРНОМ ТЕЧЕНИИ CO_2 И H_2O

Аннотация—Экспериментально и теоретически исследуется связанный лучистый и конвективный перенос в ламинарных течениях CO_2 и H_2O. Используется канал прямоугольного сечения с отношением сторон, равным 5. Стенки канала имеют однородную температуру. Для измерения профилей температуры в двух сечениях канала применяется дистанционный оптический метод на основе высокой спектральной разрешающей способности окиси углерода. Похоже, что метод позволяет получить более точные данные, чем экранированные термопары. Результаты оптических измерений хорошо согласуются с расчетами по ранее разработанной модели, в которой спектральные излучательные свойства потока газа рассчитываются по статистической модели узких полос. Совпадение теоретических результатов с экспериментальными проверено как с помощью профилей температуры, так и с помощью суммарного теплопереноса на участке между сечениями, в которых проводились измерения.